ELSEVIER

Journal of Magnetism and Magnetic Materials 131 (1994) 120–128

journal of magnetism and magnetic materials

Structure and magnetic properties of a rapidly quenched Zn–Fe–O system

Katsuhisa Tanaka *, Yoh Nakahara, Kazuyuki Hirao, Naohiro Soga

Department of Industrial Chemistry, Faculty of Engineering, Kyoto University, Sakyo-ku, Kyoto 606-01, Japan

(Received 15 July 1993)

Abstract

Crystal structure and magnetic properties of oxides in a Zn–Fe–O system prepared by the twin-roller quenching method have been examined in order to elucidate the magnetic properties of so called 'ferromagnetic amorphous oxides' in a $ZnO–Bi_2O_3–Fe_2O_3$ system, where ferrimagnetic crystals are precipitated and bring about ferromagnetic properties as revealed by the present authors. Crystalline phases with spinel structure were precipitated in all the specimens with nominal compositions of $(100-x)ZnO \cdot xFe_2O_3$ with $x = 30$ to 90 mol%. The compositional dependence of the lattice constants of these crystalline phases with the spinel structure indicates that the crystalline phases are solid solutions of Fe_3O_4 and $ZnFe_2O_4$. The specimen with $70ZnO \cdot 30Fe_2O_3$ composition where $ZnFe_2O_4$ precipitated shows magnetization of 15.6 emu/g under an external field of 10 kOe, implying that the structure of the $ZnFe_2O_4$ precipitated in this specimen is different than the normal spinel structure. The magnetization of the as-quenched specimens with $50ZnO \cdot 50Fe_2O_3$ and $30ZnO \cdot 70Fe_2O_3$ compositions decreased monotonically with an increase in heat treatment temperature. This change of magnetization is ascribed to the variation of crystal structure during the heat treatment process. Namely, the heat treatment converts the ferrimagnetic ferrites in the Zn–Fe–O system to α-Fe_2O_3 and $ZnFe_2O_4$ with normal spinel structure. The magnetic properties of the present specimens are applicable to explanation of magnetic properties of 'ferromagnetic amorphous oxides' in the $ZnO–Bi_2O_3–Fe_2O_3$ system.

1. Introduction

Magnetic properties of amorphous solids are interesting from a viewpoint of magnetism of solids where the magnetic moments are aligned randomly. As naturally anticipated from the fact that magnetic properties of crystals are intimately related to the site distribution of magnetic ions as well as crystal structure, it is thought that magnetic properties of amorphous solids are influenced by the local structure around magnetic ions and their distribution states over a long range. The present authors have been investigating the chemical structure of iron-containing amorphous solids, in particular, oxide glasses from such a standpoint [1–8]. They examined bonding characteristics of iron, the distribution of the electric field gradient around iron and iron ion clusters in oxide glasses.

Recently, amorphous oxides which show ferromagnetic properties with high Curie temperature

* Corresponding author.

SSDI 0304-8853(93)E0532-H

and relatively high magnetization were reported [9–12]. The authors argued that the ferromagnetic properties of these amorphous oxides are caused by the ferrimagnetism of microcrystals precipitated in the glass matrix because a frustration of magnetic moments inevitably takes place in amorphous oxides where magnetic moments are aligned randomly [13,14]. The authors also suggested that the smallness of the microcrystals brings about the superparamagnetic behavior in these amorphous oxides [13,14]. As for the 'ferromagnetic' $ZnO–Bi_2O_3–Fe_2O_3$ system [9,10], it was speculated that microcrystals of ferrite with spinel structure are precipitated in amorphous oxide matrix. Nonetheless, the crystal structure and magnetic properties of the microcrystalline phases have not been thoroughly clarified. It is inferred that ferrite with spinel structure in the Zn–Fe–O system precipitates in the $ZnO–Bi_2O_3–Fe_2O_3$ system. In the present investigation, an attempt was made to clarify the crystal structure and magnetic properties of oxides in the Zn–Fe–O system obtained by means of the twin-roller quenching method.

2. Experimental

Reagent-grade ZnO and Fe_2O_3 were mixed thoroughly so as to make compositions of $(100 - x)ZnO \cdot xFe_2O_3$ with $x = 30$ to 90 mol%. The mixture was calcined at 900°C for 30 min; this procedure was repeated twice. The resultant powders were pressed under a hydrostatic pressure of about 10 MPa and sintered in air at 900°C for 30 min. The sintered body was melted in an image furnace with a Xe-lamp as the heat source. The melt was quenched by being dropped onto a twin-roller made of stainless steel which was rotating at 3000 rpm. The resultant specimen was a thin foil of about 20 μm thick. The as-quenched specimens were subjected to heat treatment at 500 to 900°C for 2 h in air. The X-ray diffraction analysis with CuKα radiation was carried out for both as-quenched and heat-treated specimens in order to identify the crystalline phases precipitated and to estimate the lattice constants of the crystalline phases.

The chemical analysis was performed for some of the as-quenched specimens to determine the practical compositions of the specimens. The specimens were pulverized and dissolved in HCl aqueous solution. Then, the concentrations of zinc and iron ions were determined by means of atomic absorption spectrometry.

The magnetization and Mössbauer measurements were carried out at room temperature in order to evaluate the magnetic properties of the as-quenched and heat-treated specimens. The magnetization was determined by using a vibrating sample magnetometer. The external field was applied up to 10 kOe. The Mössbauer measurements were carried out by using 400 MBq ^{57}Co in metallic rhodium as the γ-ray source. The velocity calibration was done by using a spectrum of an α-Fe foil at room temperature.

3. Results

3.1. Crystal structure and magnetic properties of as-quenched specimens

Practical compositions of the specimens determined by the chemical analysis are shown along with the nominal compositions in Table 1. Strictly speaking, the representation of the practical composition like $65ZnO \cdot 35Fe_2O_3$ is not correct because the specimens contain Fe^{2+} as well as Fe^{3+} ions. In all the specimens examined, the concentration of ZnO in the practical composition is smaller than that in the nominal composition, presumably because of vaporization of ZnO during the melting process in the image furnace.

Table 1
Nominal and practical compositions of the present as-quenched specimens in Zn–Fe–O system. Strictly speaking, the representation of the practical composition like $65ZnO \cdot 35Fe_2O_3$ is not correct because the specimens contain Fe^{2+} as well as Fe^{3+} ions

Nominal composition [mol%]	Practical composition [mol%]
$70ZnO \cdot 30Fe_2O_3$	$65ZnO \cdot 35Fe_2O_3$
$50ZnO \cdot 50Fe_2O_3$	$43ZnO \cdot 57Fe_2O_3$
$30ZnO \cdot 70Fe_2O_3$	$24ZnO \cdot 76Fe_2O_3$
$10ZnO \cdot 90Fe_2O_3$	$7ZnO \cdot 93Fe_2O_3$

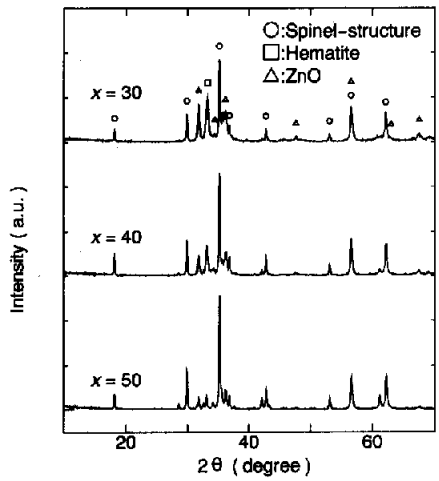

Fig. 1. X-ray diffraction patterns of $70ZnO \cdot 30Fe_2O_3$, $60ZnO \cdot 40Fe_2O_3$ and $50ZnO \cdot 50Fe_2O_3$ prepared by the twin-roller method. The assignments of the diffraction peaks are presented in the figure.

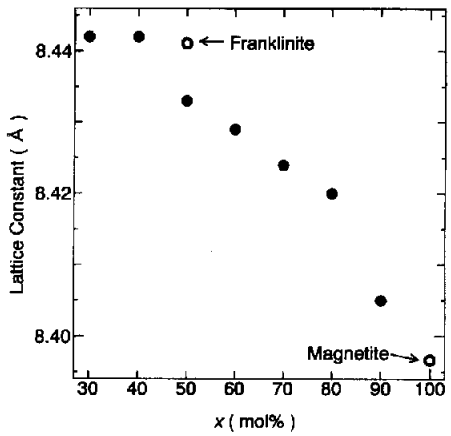

Fig. 3. The compositional dependence of lattice constant for the Zn–Fe–O system prepared by the twin-roller method. x in the abscissa denotes the concentration of Fe_2O_3. The lattice constants of Fe_3O_4 (magnetite) and $ZnFe_2O_4$ with normal spinel structure (franklinite) are also presented.

Nonetheless, since the loss of ZnO is not so large, the compositions of the specimens are hereafter represented by the nominal compositions for convenience' sake.

X-ray diffraction patterns of as-quenched $(100-x)ZnO \cdot xFe_2O_3$ with $x = 30$ to 50 and $x = 60$ to 90 are shown in Figs. 1 and 2, respectively.

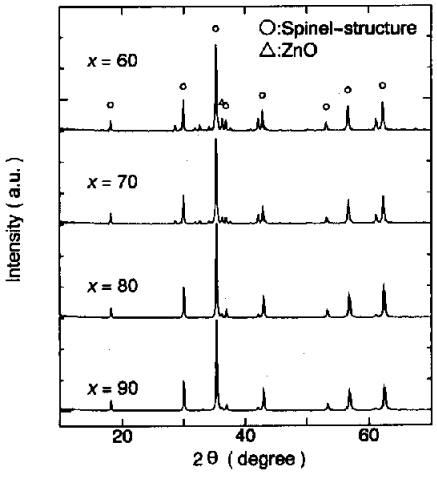

Fig. 2. X-ray diffraction patterns of $40ZnO \cdot 60Fe_2O_3$, $30ZnO \cdot 70Fe_2O_3$, $20ZnO \cdot 80Fe_2O_3$ and $10ZnO \cdot 90Fe_2O_3$ prepared by the twin-roller method. The assignments of the diffraction peaks are presented in the figure.

Crystalline phases with spinel structure are observed in all the specimens, although the intensity of the diffraction peaks varies with composition. Only the diffraction peaks assigned to crystal with spinel structure are observed in the specimen with $10ZnO \cdot 90Fe_2O_3$ composition. In the as-quenched specimens with other compositions, α-Fe_2O_3 (hematite) and ZnO were precipitated in addition to the crystalline phases with spinel structure. As the concentration of Fe_2O_3 in the specimens decreases, the intensity of the diffraction peaks of α-Fe_2O_3 and ZnO increases. From the positions of diffraction peaks of the crystal with spinel structure, lattice constants were evaluated. The compositional dependence of the lattice constant for the crystal with spinel structure is shown in Fig. 3. The lattice constants of Fe_3O_4 (magnetite) and $ZnFe_2O_4$ (franklinite), cited from the Powder Diffraction File compiled by JCPDS (Joint Committee on Powder Diffraction Standards), are also shown. The lattice constants of the crystals with spinel structure in the specimens with $70ZnO \cdot 30Fe_2O_3$ and $60ZnO \cdot 40Fe_2O_3$ compositions are almost identical with that of franklinite. The lattice constant decreases monotonically with an increase in the concentration of Fe_2O_3, and approaches the lattice constant of magnetite.

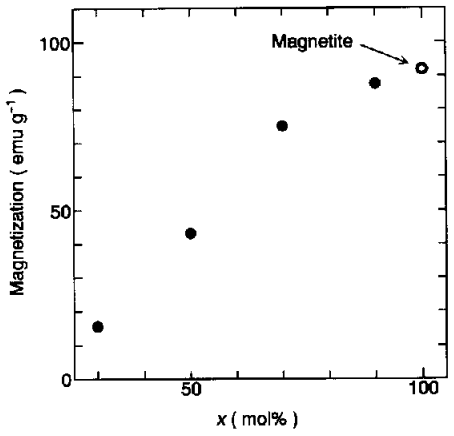

Fig. 4. The compositional dependence of magnetization at room temperature for the Zn–Fe–O system prepared by the twin-roller method. The magnetization of Fe_3O_4 is also presented.

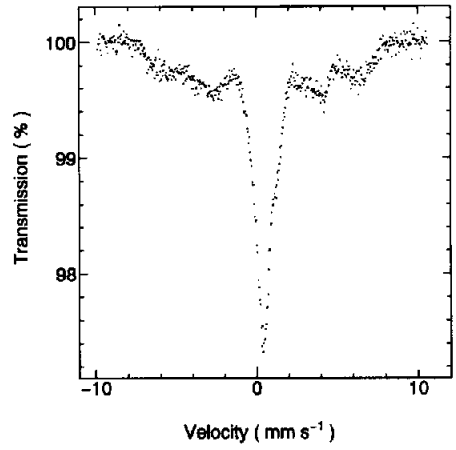

Fig. 5. Room temperature Mössbauer spectrum of $50ZnO \cdot 50Fe_2O_3$ prepared by the twin-roller method.

Fig. 4 shows the compositional dependence of magnetization at room temperature. The magnetization of magnetite is also shown in this figure. The magnetization increases monotonically with an increase in concentration of Fe_2O_3, and approaches the value of magnetite. It should be noted that the magnetization of $70ZnO \cdot 30Fe_2O_3$, where a ferrite with lattice constant similar to that of $ZnFe_2O_4$ precipitates, is relatively high. Since $ZnFe_2O_4$ with normal spinel structure is antiferromagnetic with a Néel temperature of about 10 K [15], the structure of the ferrite precipitated in the specimen with $70ZnO \cdot 30Fe_2O_3$ composition is different than the normal spinel structure.

Room temperature Mössbauer spectra of as-quenched $50ZnO \cdot 50Fe_2O_3$ and $10ZnO \cdot 90Fe_2O_3$ are shown in Figs. 5 and 6, respectively. The Mössbauer spectrum of the $50ZnO \cdot 50Fe_2O_3$ is composed of paramagnetic and ferromagnetic components. The ferromagnetic component manifests very broad linewidths. The intense paramagnetic absorption peak around 0.4 mm/s is attributed to Fe^{3+} ions. A close look at Fig. 5 reveals that a weak absorption is observed around 1.3 mm/s as a shoulder of the intense paramagnetic peak. This absorption is assigned to Fe^{2+} ions. The Mössbauer spectrum of the as-quenched $10ZnO \cdot 90Fe_2O_3$ shown in Fig. 6 is similar to that of magnetite [16–18].

3.2. *Crystal structure and magnetic properties of heat-treated specimens*

The variation of X-ray diffraction pattern with heat treatment temperature for the $50ZnO \cdot 50Fe_2O_3$ is shown in Fig. 7. The diffraction pattern does not change so largely with heat treatment, although the intensity of diffraction peaks of ZnO which precipitates as a minor phase in the as-quenched specimen decreases with an in-

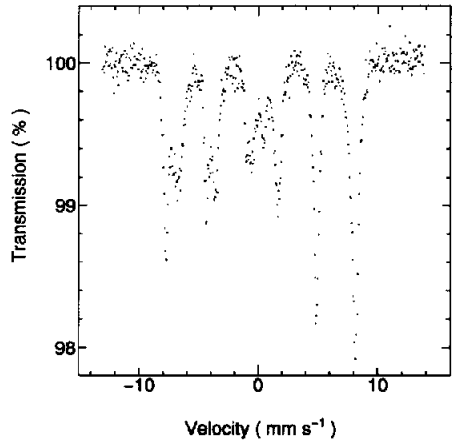

Fig. 6. Room temperature Mössbauer spectrum of $10ZnO \cdot 90Fe_2O_3$ prepared by the twin-roller method.

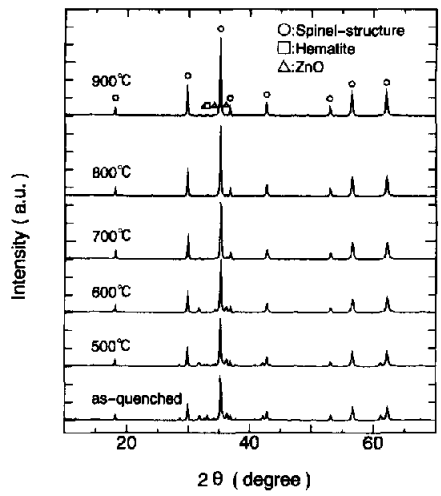

Fig. 7. Variation of X-ray diffraction pattern with heat treatment temperature for $50ZnO \cdot 50Fe_2O_3$. The X-ray diffraction pattern of as-quenched specimen is also presented.

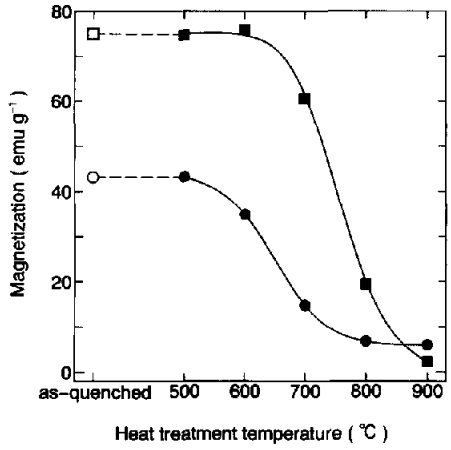

Fig. 9. Variation of magnetization with heat treatment temperature for $50ZnO \cdot 50Fe_2O_3$ and $30ZnO \cdot 70Fe_2O_3$. The circles and squares denote the magnetizations of $50ZnO \cdot 50Fe_2O_3$ and $30ZnO \cdot 70Fe_2O_3$, respectively. The open symbols represent the as-quenched specimens. The solid and broken curves are to guide eyes.

crease in the heat treatment temperature. The average crystallite size of the ferrite with spinel structure estimated from the full width at half maximum of the diffraction peaks is about 25 nm, which is independent of the heat treatment temperature. Fig. 8 shows the dependence of X-ray diffraction pattern of the specimen with $30ZnO \cdot 70Fe_2O_3$ composition on the heat treatment temperature. In this case, the intensity of the diffraction peaks of hematite increases with an increase in heat treatment temperature. The diffraction peaks of crystalline phases with spinel structure are observed in all the heat-treated specimens with this composition.

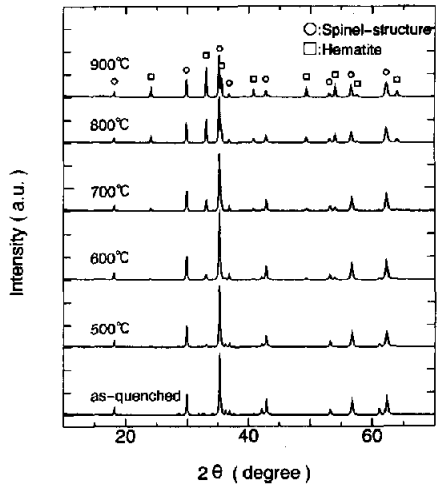

Fig. 8. Variation of X-ray diffraction pattern with heat treatment temperature for $30ZnO \cdot 70Fe_2O_3$. The X-ray diffraction pattern of as-quenched specimen is also presented.

Fig. 9 shows the variations of magnetization with heat treatment temperature for the specimens with $50ZnO \cdot 50Fe_2O_3$ and $30ZnO \cdot 70Fe_2O_3$ compositions. The circles and squares in the figure correspond to $50ZnO \cdot 50Fe_2O_3$ and $30ZnO \cdot 70Fe_2O_3$, respectively. The magnetization of as-quenched specimens, which is represented by the open symbols, is also shown. The magnetizations of the specimens heat-treated at 500 and 600°C are almost the same as the magnetization of as-quenched specimens for both $50ZnO \cdot 50Fe_2O_3$ and $30ZnO \cdot 70Fe_2O_3$ compositions. The magnetization decreases monotonically with an increase in heat treatment temperature; in particular, it decreases drastically when the heat treatment temperature is above 600°C. For the specimens heat-treated at 900°C, the magnetization is rather small.

The room temperature Mössbauer spectrum of the $50ZnO \cdot 50Fe_2O_3$ specimen heat-treated at 600°C is shown in Fig. 10. The spectrum is similar

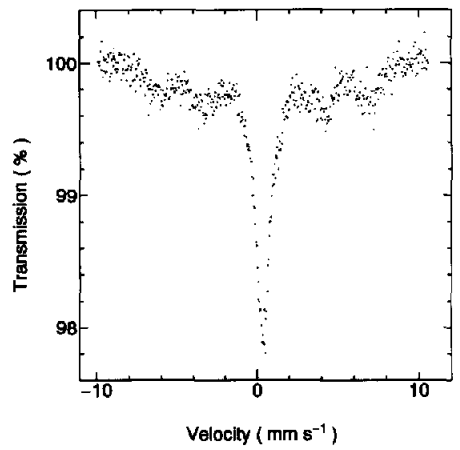

Fig. 10. Room temperature Mössbauer spectrum of $50ZnO \cdot 50Fe_2O_3$ heat-treated at 600°C.

to that of the as-quenched specimen shown in Fig. 5, although the shoulder in the paramagnetic absorption peak, which is observed in the as-quenched specimen, disappears in the heat-treated specimen. This means that the Fe^{2+} ions are oxidized by the heat treatment. Fig. 11 shows the room temperature Mössbauer spectrum of the specimen heat-treated at 700°C. When compared with the spectrum of the specimen heat-treated at 600°C, the fraction of ferromagnetic component is smaller. This is coincident with the dependence of magnetization on the heat treatment temperature shown in Fig. 9; the magnetization decreases drastically when the heat treatment temperature varies from 600 to 700°C.

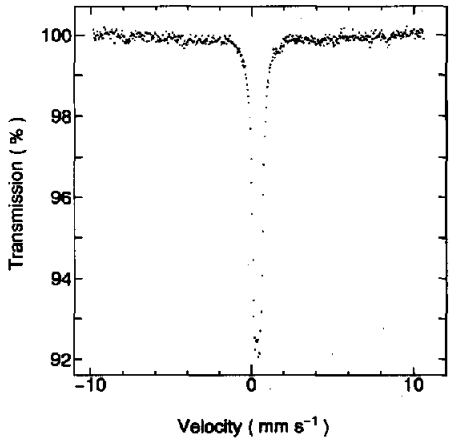

Fig. 11. Room temperature Mössbauer spectrum of $50ZnO \cdot 50Fe_2O_3$ heat-treated at 700°C.

4. Discussion

The X-ray diffraction analyses indicate that the main phase precipitated in the as-quenched Zn–Fe–O system is crystal with spinel structure. From the compositional dependence of the lattice constant of the crystal with spinel structure shown in Fig. 3, it is found that the precipitated phases are solid solutions of $ZnFe_2O_4$ with magnetite. In this case, the $ZnFe_2O_4$ does not have normal spinel structure because the as-quenched $70ZnO \cdot 30Fe_2O_3$ specimen, where ferrite with $ZnFe_2O_4$ composition precipitates, possesses magnetization of 15.6 emu/g under the external field of 10 kOe, as shown in Fig. 4. One possible mechanism which explains the magnetization of the $ZnFe_2O_4$ is related to the presence of Fe^{2+}. It is known that Zn^{2+} ions much more favorably occupy the tetrahedral sites in the spinel structure because of the sp^3 hybrid orbital of Zn^{2+} ion [19]. Hence, a large part of Fe^{3+} and Fe^{2+} ions occupy the octahedral sites, and superexchange interaction among Fe^{3+} and Fe^{2+} ions in the octahedral sites brings about the ferrimagnetism. Another possible structure of $ZnFe_2O_4$ precipitated in the present specimens during the rapidly quenching process is shown in Fig. 12. It is assumed that in the as-quenched specimen, some of the Zn^{2+} ions occupy the octahedral sites and some of the Fe^{3+} and/or Fe^{2+} ions take tetrahedral sites in $ZnFe_2O_4$. The left figure in Fig. 12 represents the spinel structure where one Zn^{2+} ion in tetrahedral site is exchanged for one Fe^{3+} ion in octahedral site. Since the superexchange interaction is stronger for the bond angle of 180° than for the bond angle of 90°, the superexchange interaction between Fe^{3+} ion in tetrahedral site and Fe^{3+} ion in octahedral sites governs the direction of each magnetic moment. When the magnetic moment of the Fe^{3+} ion in the tetrahedral site is down as shown in Fig. 12, the magnetic moments of the other three Fe^{3+} ions in the octahedral sites are up, so that two magnetic moments parallel to each other yield the net

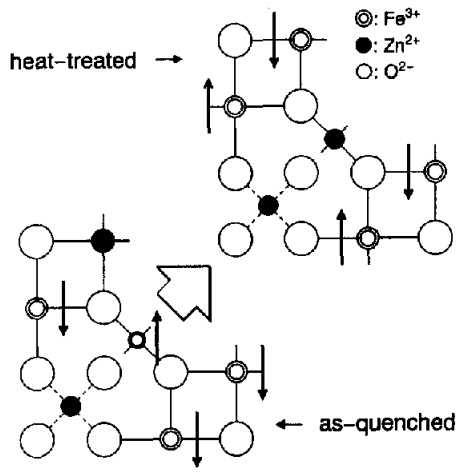

Fig. 12. Possible structural change of $ZnFe_2O_4$ precipitated in the as-quenched specimens ($70ZnO \cdot 30Fe_2O_3$ and $60ZnO \cdot 40Fe_2O_3$) with heat treatment.

magnetic moment. As a result, ferrimagnetism arises. Although the number of Zn^{2+} ions in octahedral sites may be small because of the fact that Zn^{2+} ions are much more favorably apt to occupy tetrahedral sites, this structure is possible because a high temperature form, which prefers disordered structure owing to the effect of entropy, can be quenched in the present specimen. It is speculated that not only the superexchange interaction between Fe^{3+} and Fe^{2+} ions in the octahedral sites but also the site exchange between Zn^{2+} and iron ions result in the existence of magnetization in $ZnFe_2O_4$ precipitated in the present specimens.

On the other hand, heat treatment leads to a stable crystal structure, i.e., a normal spinel structure for $ZnFe_2O_4$, which is illustrated on the right side in Fig. 12. In the $ZnFe_2O_4$ with normal spinel structure, as well known, the magnetic moments are ordered antiferromagnetically due to the superexchange interaction among Fe^{3+} ions in the octahedral sites. Furthermore, the heat treatment leads to a decomposition of the ferrite solid solution between magnetite and ferrimagnetic $ZnFe_2O_4$ into α-Fe_2O_3 and $ZnFe_2O_4$, as shown in Fig. 8. The $ZnFe_2O_4$ formed by the decomposition of the ferrimagnetic ferrite is thought to have the normal spinel structure. Hence, the magnetization decreases with an increase in heat treatment temperature for as-quenched specimens with $50ZnO \cdot 50Fe_2O_3$ and $30ZnO \cdot 70Fe_2O_3$ compositions.

The intense paramagnetic peaks are observed in the Mössbauer spectrum of the as-quenched $50ZnO \cdot 50Fe_2O_3$ as shown in Fig. 5 although this specimen shows high magnetization such as 43.2 emu/g under an external field of 10 kOe (see Fig. 4). Also, the Mössbauer spectrum of this specimen manifests broad absorption lines split due to hyperfine fields. Dobson et al. [20] carried out Mössbauer spectroscopy for $Zn_yFe_{3-y}O_4$ with $0 \leq y \leq 1$ and revealed that the linewidth of the hyperfine spectrum becomes broader as y increases. For $y = 0.6$, a quadrupole splitting pattern was observed in addition to the hyperfine spectrum. They attributed the broad linewidths of the hyperfine spectra to the variation of number of iron ions in tetrahedral sites which are nearest neighbors to Fe^{3+} ions in octahedral sites, because Zn^{2+} and Fe^{3+} are distributed randomly in the tetrahedral sites [20]. In the present case, the broadness of the linewidth is similarly ascribed to the site distribution of iron ions within one ferrite crystalline particle. In the as-quenched $50ZnO \cdot 50Fe_2O_3$ specimen, i.e., the specimen with a practical composition of $43ZnO \cdot 57Fe_2O_3$, Fe^{3+} and Fe^{2+} ions are distributed in both tetrahedral and octahedral sites and most of the Zn^{2+} ions occupy tetrahedral sites. The distribution of number of iron ions in tetrahedral sites which magnetically interact with iron ions in octahedral sites primarily contributes to the broadness of the linewidth. Furthermore, the high concentration of diamagnetic Zn^{2+} ions brings about a frustration of some magnetic moments of iron ions. In other words, one ferrite particle is divided into several magnetic clusters in which all of the magnetic moments on the Fe^{3+} and Fe^{2+} ions are correlated with each other over a long range, and there exists a frustration of magnetic moments in the boundary between clusters. These clusters have different magnetic transition temperatures, in this case superparamagnetic blocking temperatures, from each other, because the compositions and sizes of the clusters are different from each other. A wide distribution of magnetic transition

temperatures leads to a broad distribution of hyperfine fields at room temperature, and hence, the hyperfine spectrum manifests very broad linewidths. It is inferred that the paramagnetic peaks in the Mössbauer spectrum are caused by both paramagnetic clusters with a structure similar to the normal spinel $ZnFe_2O_4$ and superparamagnetic clusters with sufficiently small size. A hyperfine spectrum with broad linewidth similar to that of the present as-quenched $50ZnO \cdot 50Fe_2O_3$ was also observed for $20ZnO \cdot 30Bi_2O_3 \cdot 50Fe_2O_3$, prepared by the water-cooling method [21,22]. It is speculated that the crystalline phases with similar structure to the present ferrite solid solution are precipitated in the water-cooled $20ZnO \cdot 30Bi_2O_3 \cdot 50Fe_2O_3$ and yield a similar Mössbauer spectrum.

Dobson et al. [20] also reported that the Mössbauer spectra of $Zn_yFe_{3-y}O_4$ with $y \geq 0.8$ are composed of only quadrupole doublet. By contrast, for the present as-quenched specimen with $50ZnO \cdot 50Fe_2O_3$ composition, the practical composition of which is $43ZnO \cdot 57Fe_2O_3$, i.e., $y = 0.82$, the hyperfine spectrum was observed in addition to the paramagnetic peak. This difference is due to the presence of Fe^{2+} ions and the possible occupation of octahedral sites by some Zn^{2+} ions in the present as-quenched specimen.

The experimental results presented here can be applied to the elucidation of magnetic properties of 'ferromagnetic amorphous oxides' in the $ZnO–Bi_2O_3–Fe_2O_3$ system. It is speculated that microcrystalline phases of solid solutions of Fe_3O_4 with ferrimagnetic $ZnFe_2O_4$ precipitated in the amorphous oxides of the $ZnO–Bi_2O_3–Fe_2O_3$ system during the preparation process. These microcrystalline phases lead to the ferromagnetic behavior of the amorphous oxides under a high external field such as 10 kOe. The Curie temperature of the amorphous $20ZnO \cdot 30Bi_2O_3 \cdot 50Fe_2O_3$, i.e. 450 K [9,10], is plausible for the ferrite compounds with spinel structure. The presence of diamagnetic Zn^{2+} ions makes the Curie temperature lower than those of other ferrites with spinel structure such as Fe_3O_4, $MnFe_2O_4$ and $CoFe_2O_4$. The microcrystals were too small to detect by means of X-ray diffraction with CuKα radiation [10]. The smallness of the microcrystals brought about the superparamagnetic behavior in the Mössbauer spectra [10].

5. Conclusion

The crystal structure and magnetic properties of oxides in a Zn–Fe–O system prepared by the twin-roller quenching method were examined by using X-ray diffraction, magnetization measurements and Mössbauer spectroscopy. The main phases precipitated in the as-quenched specimens have spinel structure, and the compositional dependence of lattice constant indicated that these crystals are solid solutions between Fe_3O_4 and $ZnFe_2O_4$. The as-quenched $70ZnO \cdot 30Fe_2O_3$ specimen which contains the $ZnFe_2O_4$ possesses magnetization of 15.6 emu/g at room temperature. This magnetic behavior of the $ZnFe_2O_4$ was explained in terms of the superexchange interaction between Fe^{3+} and Fe^{2+} ions in octahedral sites as well as the magnetic structure brought about by the site exchange of Zn^{2+} in tetrahedral sites with Fe^{3+} and/or Fe^{2+} in octahedral sites. The magnetization of the as-quenched specimen increased monotonically with an increase in concentration of iron, and approached the value of Fe_3O_4. It is concluded that microcrystalline phases of the present solid solutions of ferrites precipitate in the so called 'ferromagnetic amorphous oxides' of the Zn–Bi–Fe–O system.

6. Acknowledgement

The present authors would like to thank Dr. Y. Isozumi of Institute for Chemical Research, Kyoto University, and Dr. S. Ito of Radioisotope Research Center, Kyoto University for the Mössbauer measurements. The authors would like to thank Mr. H. Miyazaki of Ishihara Sangyo Co. Ltd. for the magnetization measurements. The authors are also indebted to Prof. H. Takatsuki, Environment Preservation Center, Kyoto University for atomic absorption spectrometry. This work was financially supported by a Grant-in-Aid for Encouragement of Young Scientists (No. 04750670).

7. References

[1] K. Tanaka, K. Hirao and N. Soga, J. Non-Cryst. Solids 85 (1986) 228.
[2] K. Tanaka and N. Soga, J. Non-Cryst. Solids 95&96 (1987) 255.
[3] K. Tanaka, K. Kamiya, T. Yoko, S. Tanabe, K. Hirao and N. Soga, J. Non-Cryst. Solids 109 (1989) 289.
[4] K. Tanaka, T. Ishihara, K. Hirao and N. Soga, J. Ceram. Soc. Jpn. 101 (1993) 273.
[5] K. Tanaka, K. Hirao and N. Soga, Nucl. Instr. Meth. B 76 (1993) 105.
[6] K. Tanaka, K. Kamiya, T. Yoko, S. Tanabe, K. Hirao and N. Soga, Phys. Chem. Glasses 32 (1991) 16.
[7] K. Tanaka, N. Soga, K. Hirao and K. Kimura, J. Appl. Phys. 60 (1986) 728.
[8] K. Tanaka, K. Hirao and N. Soga, J. Appl. Phys. 64 (1988) 3299.
[9] N. Ota, M. Okubo, S. Masuda and K. Suzuki, J. Magn. Magn. Mater. 54–57 (1986) 293.
[10] K. Suzuki, H. Onodera, M. Sakurai, S. Masuda, A. Matsumoto and H. Sadamura, IEEE Trans. Magn. 22 (1986) 1090.
[11] S. Nakamura and N. Ichinose, J. Non-Cryst. Solids 95&96 (1987) 849.
[12] Y. Nagata, T. Inoh and K. Ohta, IEEE Trans. Magn. 23 (1987) 2317.
[13] K. Tanaka, K. Hirao and N. Soga, J. Appl. Phys. 69 (1991) 7752.
[14] K. Tanaka, K. Hirao, N. Soga and H. Mori, Jpn. J. Appl. Phys. 30 (1991) L2095.
[15] S. Chikazumi, Physics of Ferromagnetism (Syokabo, Tokyo, 1978).
[16] B.J. Evans and S.S. Hafner, J. Appl. Phys. 40 (1969) 1411.
[17] W. Kündig and R.S. Hargrove, Solid State Commun. 7 (1969) 223.
[18] M. Robbins, G.K. Wertheim, R.C. Sherwood and D.N.E. Buchanan, J. Phys. Chem. Solids 32 (1971) 717.
[19] E.J.W. Verwey and E.L. Hailmann, J. Chem. Phys. 15 (1947) 174.
[20] D.C. Dobson, J.W. Linnett and M.M. Rahman, J. Phys. Chem. Solids 31 (1970) 2727.
[21] K. Tanaka, K. Hirao and N. Soga, The Physics of Non-Crystalline Solids, eds. L.D. Pye, W.C. LaCourse and H.J. Stevens (Taylor & Francis, London, 1992), p. 296.
[22] K. Tanaka, K. Hirao and N. Soga, Ferrites: Proceedings of The Sixth International Conference on Ferrites (The Japan Society of Powder and Powder Metallurgy, Tokyo and Kyoto, 1992), p. 1003.